Available online at www.sciencedirect.com
SCIENCE DIRECT®
International Journal of Heat and Mass Transfer 47 (2004) 3659–3667
International Journal of HEAT and MASS TRANSFER
www.elsevier.com/locate/ijhmt

Photographic study of bubble behaviors in forced convection subcooled boiling

Rong Situ [a,*], Ye Mi [a,1], Mamoru Ishii [a], Michitsugu Mori [b]

[a] School of Nuclear Engineering, Purdue University, 400 Central Drive, West Lafayette, IN 47907-2017, USA
[b] Tokyo Electric Power Company, 4-1 Egasaki-cho, Tsurumi-ku, Yokohama 230-8510, Japan

Received 6 June 2003; received in revised form 6 April 2004

Abstract

Forced convection subcooled water boiling experiments were conducted in a vertical annular channel. A high-speed digital video camera was applied to record the dynamics of the subcooled boiling process. The flow visualization results show that the bubble departure frequency generally increases as the heat flux increases. For some cases, the departure frequency may reach a limit around 1000 bubbles/s. In addition, bubble lift-off diameter, bubble growth rate and bubble velocity after bubble lift-off were determined by analyzing the images. The experimental data obtained from this study can be used in modeling the bubble departure frequency, bubble lift-off diameter, and bubble dynamics in forced convection subcooled boiling.

Keywords: Bubble; Flow visualization; Subcooled boiling; Two-phase flow; Forced convection

1. Introduction

The subcooled boiling region is characterized, in convective flow boiling, as boiling occurring close to the wall while the remaining bulk of the fluid is subcooled. Bubbles will be rapidly condensed if they move out of the developing saturation boundary. In the subcooled region, there exists a small void fraction. Gradually, as the bulk is heated by conduction and convection, the saturation boundary expands and eventually covers the entire channel. At this point fully developed nucleate boiling occurs and bubbles may exist anywhere in the channel. The subcooled boiling region is important for boiling water reactor (BWR) due to the following reasons. First, bubbles generated in subcooled boiling region affect the downstream boiling and void distribution. Secondly, subcooled boiling determines the two-phase characteristics that will exist in the downstream of the core channel. Furthermore, the subcooled region can also be responsible for developing flow instabilities in a BWR because of the strong coupling between the void fraction and the neutron moderation in the reactor core. Finally, the density wave instability is also sensitive to the motion of the boiling boundary, because it defines the vapor source that propagates downstream.

Currently, the two-fluid model [1] as well as the interfacial area transport equation [2] and/or the bubble number density transport equation [3,4] can offer an advanced analysis for nuclear reactor systems. Several parameters, such as nucleation site density, bubble departure size and frequency, are required to be modeled as boundary conditions in the transport equations.

The bubble departure frequency and departure size in pool boiling have been studied extensively by various researchers [5,6]. However, in forced convection subcooled boiling, the nucleation cycle becomes more complex and stochastic because of the bulk turbulent convection. Many experimental investigations have been conducted to determine the point of net vapor

* Corresponding author. Tel.: +1-765-494-5759; fax: +1-765-494-9570.
E-mail address: situ@ecn.purdue.edu (R. Situ).
[1] Current address: En'Urga Inc., 1291 Cumberland Ave., West Lafayette, IN 47906, USA.

0017-9310/$ - see front matter © 2004 Elsevier Ltd. All rights reserved.
doi:10.1016/j.ijheatmasstransfer.2004.04.005

Nomenclature

A	liquid flow area
D_b	bubble diameter
D_{lo}	bubble lift-off diameter
D_d	bubble departure diameter
F_d	bubble departure frequency
G	mass flux
l_h	heated length
N_{sub}	subcooling number
N_{Zu}	Zuber number (phase change number)
q''_w	wall heat flux
T_{sat}	saturation temperature
y	distance from wall
z_d	distance from start of heated section to the specific nucleation site

Greek symbols

Δi_{fg}	latent heat of vaporization
$\Delta i_{sub,in}$	Inlet liquid subcooling enthalpy
$\Delta\rho$	liquid and vapor density difference
ρ_v	mass density of vapor phase
ρ_f	mass density of liquid phase
σ	surface tension
ζ_h	heated perimeter

Superscript

+	non-dimensional parameter

generation (NPVG) and to measure the void fraction. The exiting data can be divided into two groups: low pressure and high pressure data. These data were summarized by Rogers et al. [7] and Lee and Bankoff [8].

Many researchers attempted to visually quantify parameters important to the bubble nucleation cycle. Gunther [9] carried out a high-speed photographic study on the nucleate boiling process in forced convection flow of water. Bubble growth and condensation curves in the subcooled region were measured. Unal [10] measured the maximum bubble diameters at the incipient point of boiling. A correlation was obtained based on his data and the data from literature in the pressure range from 0.1 to 15.9 MPa. Recently, Zeitoun et al. [11] measured the bubble size and surface area by using high-speed photography and digital image processing techniques. Kandlikar and Stumm [12] measured the bubble departure diameter and contact angle in horizontal convective subcooled boiling of water. Thorncroft et al. [13] visually investigated the vapor bubble growth and departure in vertical up-flow and down-flow forced convection boiling of FC-87. The authors found that for upward flow, bubbles slide along the heater wall rather than lift-off from the wall when they depart from the nucleation cavities. Warrier et al. [14] measured the bubble diameter and bubble collapse rate in the bulk region.

Although many researches have been conducted on subcooled flow boiling, some fundamental parameters, such as bubble departure frequency, bubble lift-off diameter, have not been addressed sufficiently. The purpose of this study is to experimentally investigate the bubble nucleation cycle in forced convection subcooled boiling with upward flow. Flow visualization was performed under subcooled boiling in an experimental facility by using water as the working fluid. Detailed phenomena, such as bubble growth, condensation, coalescence and sliding, were clearly observed from the high-speed digital video images. The bubble departure frequency, bubble lift-off diameters and bubble dynamics after lift-off were obtained by analyzing the images.

2. Experimental facility and setup

An experimental facility has been designed to measure the relevant two-phase parameters necessary for developing constitutive models for the two-fluid model in subcooled boiling. The experimental facility is a scaled-down loop from a prototypic BWR based on proper scaling criteria for geometric, hydrodynamic, and thermal similarities [15]. The experimental facility and flow visualization system are described in this section.

2.1. Experimental facility

The basic flow path (shown in Fig. 1) and description of the experimental facility are given in this section. The subcooled water is held in the main tank. The main tank has a cartridge heater and heat exchanger to control the test-section-inlet subcooling. The water is pumped by a positive displacement pump and divided into four separate lines. Each line runs to a fitting that is connected to the bottom of the test section. The test section is an annulus formed by a clear polycarbonate tube on the outside with an ID of 38.1 mm, and a cartridge heater on the inside with an OD of 19.1 mm.

The inlet and outlet fluid temperature and pressure drop cross the test section are measured by K-type thermocouples and Honeywell ST 3000 Smart Transmitter, respectively. The corrected errors of the thermocouples are ±1.0 °C, and the combined zero and span

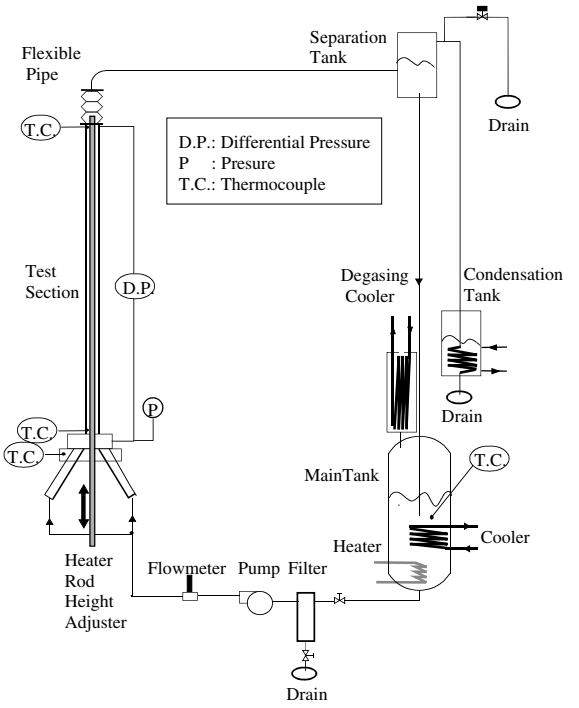

Fig. 1. Schematic diagram of experimental facility.

inaccuracy for the differential pressure cell is ±0.4% of span.

The heater has an overall length of 2670 mm with a heated section of 1730 mm in length. The maximum power of the heater is 20 kW that corresponds to a maximum heat flux of 0.193 MW/m^2. At the top of the test section, an expansion joint is installed to accommodate the thermal expansion of the polycarbonate test section. A separator tank is used to separate vapor phase from water. The steam is then condensed, and the water is returned to the main tank. The separator tank is located directly above the main tank.

2.2. Experimental setup of flow visualization

The setup of the flow visualization system is described in Fig. 2. A CCD camera is mounted on the back of a magnification-changeable bellow with a C-mount, and a Micro-NIKKOR 105 mm 1:2.8 lens is mounted in front of the bellow. The camera is placed on a 1-D traverse rail that can be moved forward or backward relative to the test in a certain range. The 1-D traverse rail is placed on a 2-D traverse system that can be moved vertically (5.0 cm) and laterally (11.4 cm). This forms a 3-D traverse system. An image box is installed on the test section to minimize the image distortion since the front side of the image box (close to the camera) is filled with water. The side surface of the image box is covered by black paper to avoid any sidelight. Two 300 W GE

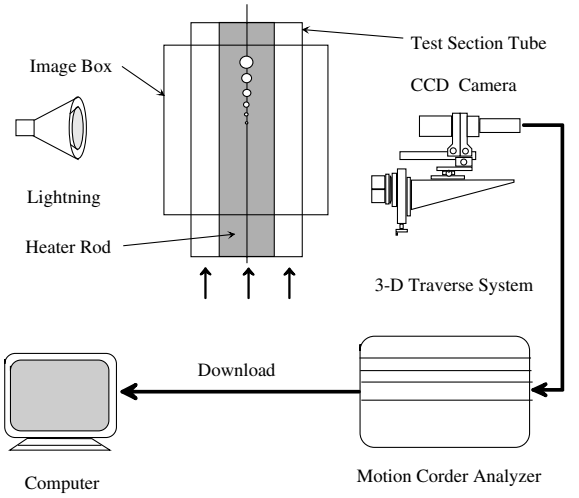

Fig. 2. Experimental setup of flow visualization.

spotlights, supported by adjustable arms, are located behind the image box to provide lighting for the flow visualization.

In preparing for an experiment, the water in the main tank was degassed by heating up the tank for 24 h. Before an experiment measurement, the flow reached steady state, and the inlet temperature and fluid velocity kept constant for 30 min. The high-speed video camera was adjusted to focus on an active nucleation site. In order to capture the very short bubble-growth period, i.e., only a few milliseconds, the camera frame rate was set as high as 5000 frame/s (fps), and the resolution of each image was 80×128 pixels. The distance between adjacent pixels is 11 μm. The maximum frame rate of the Motion Corder Analyzer, 10,000 fps, was not used because the image size is only 128×34 pixels, which is not enough to provide a reasonable image resolution. By adjusting the magnification ratio of the camera, a whole nucleation site along with a certain downstream distance can be covered. For each recording, a total of 13,104 frames of pictures, i.e. 2.6 seconds' images, were taken by the video camera and downloaded to a computer. In general, one recording was made for each flow condition in the current experiments.

3. Results and discussion

3.1. Experimental conditions

Six runs of experiments have been performed. Each run includes several test points. The inlet temperature, fluid velocity, and the nucleation site remain unchanged while the heat flux increases. The experimental conditions are listed in Table 1. In Table 1, "z_d" shows the distance from the start of heat section to the nucleation

Table 1
Experimental conditions

Run	T_{in} (°C)	q'' (kW/m^2)	G (kg/m^2 s)	z_d (m)
1	93.4	61.8–73.3	497.0	1.118
2	95.4	61.8–90.7	570.0	1.118
3	93.4	79.1–90.7	570.0	1.180
4	93.4	84.9–108	570.0	1.213
5	98.0	61.8–90.7	570.0	0.535
6	98.0	54.0–90.7	570.0	0.936

site. The nucleation site in Runs 1 and 2 is the same site. The nucleation sites more downstream from point of onset of nucleate boiling (ONB) are coved by adjacent bubbles and not easy to observe. The present study is to observe the bubble departure/lift-off phenomena rather than to build a database for the modeling of bubble departure/lift-off parameters. Therefore, only nucleation sites at the beginning of the nucleation boiling were observed. In the future research, more test conditions will be performed and more nucleation sites will be observed to establish a solid database.

In the test conditions, the fluid velocities were set to be relatively low, i.e., around 0.5 m/s. These fluid velocities were not a scaled quantity from prototype BWR, which should be 2.0 m/s. The choosing of these fluid velocities is due to two reasons: First, a steady active nucleation site is easy to find; secondly, the purpose of this research is to observe bubble behaviors in a large range of test conditions, not necessary the condition scaled from BWR.

As shown in Table 1, the observed nucleation site positions at higher inlet temperature, for example, 98.0 °C, are more upstream than those at lower inlet temperature. This is because, for the cases of high inlet temperature, nucleation sites at downstream locations were covered by passing bubbles coming from upstream nucleation sites and were not easy to be observed.

Fig. 3 shows the test points in the subcooling number vs. local Zuber number coordinates. The definitions of the subcooling number and Zuber number, or phase change number, are

$$N_{sub} = \frac{\Delta i_{sub,in}}{\Delta i_{fg}} \frac{\Delta \rho}{\rho_v} \tag{1}$$

and

$$N_{Zu} = \frac{q''_w \zeta_h z_d}{A v_{fi} \Delta i_{fg}} \frac{\Delta \rho}{\rho_v \rho_f} \tag{2}$$

where $\Delta i_{sub,in}$, Δi_{fg}, $\Delta \rho$, q''_w, ζ_h, A, and v_{fi} are inlet liquid subcooling enthalpy, latent heat of vaporization, liquid and vapor density difference, wall heat flux, heated perimeter, liquid flow area, and inlet liquid velocity, respectively. Note that the heated length in Eq. (2) is distance from the start of heat section to the nucleation site instead of the whole heated length.

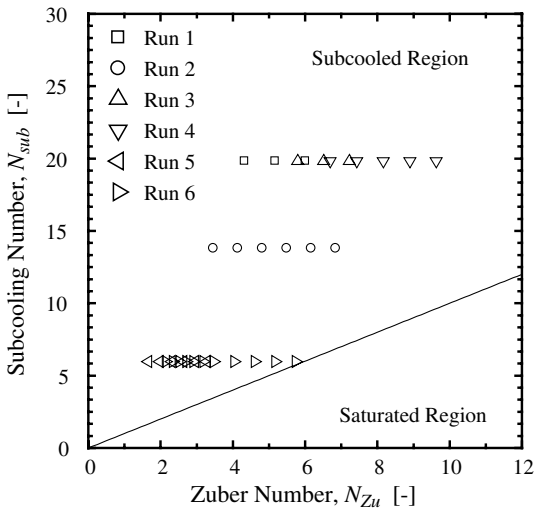

Fig. 3. Test pointers in the subcooling number–Zuber number coordinates.

In Fig. 3, the bulk temperatures at the location nucleation site all of the test points are in the subcooled region. For each run, the subcooling numbers of all the test points are the same since the inlet temperature and inlet velocity do not change. The only difference among these test points is the heat flux, which is represented by the Zuber number.

3.2. Results of bubble departure frequency

The bubble departure frequencies were counted by replaying the video images. By analyzing the recorded images, it was found that two different nucleation phenomena exist. The nucleation sites in Runs 1, 2, and 5 belong to the first one, where the waiting periods are very short, or even unnoticeable, that is, when a bubble departs from a nucleation site, the following bubble appears almost simultaneously. On the other hand, the nucleation sites in Runs 3 and 4 are the other one that have relatively apparent and longer waiting periods. When a bubble departs from the nucleus cavity, its cavity is then re-covered by liquid, and, the next bubble will appear after a certain time interval. The nucleation

site in Run 6 seems to be a transition between these two kinds of nucleation phenomena.

The results of the bubble departure frequency are plotted against the Zuber number in Fig. 4. The departure frequencies of the first kind of nucleation site are higher than 300 bubbles/s, while the departure frequencies of the second kind of nucleation site are lower than 300 bubbles/s, as shown in Fig. 4. The bubble growth period under all these conditions is short, less than 3 ms. Accordingly, the bubble waiting period dominates the total bubble departure period. For the transition between these two kinds of nucleation phenomena, i.e., Run 6, when the heat flux is small, the waiting period is relatively long and the departure frequency is very low. As the heat flux increases, the departure frequency increases significantly. When the heat flux reaches 59.3 kW/m^2, the departure frequency jumps to 861 bubbles/s. As the departure frequency increases, the waiting period decreases. When the departure frequency is very high, the waiting period becomes very short, or even unnoticeable.

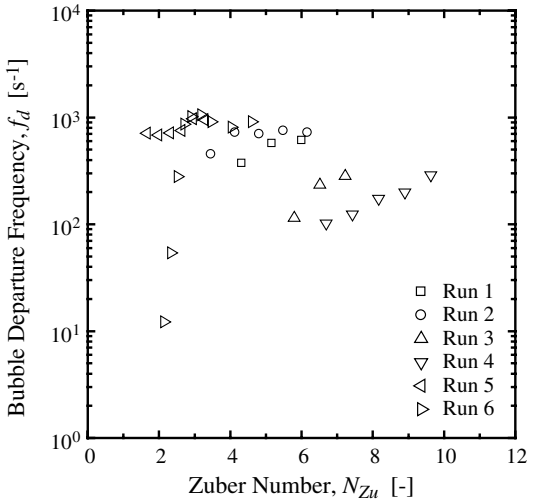

Fig. 4. Results of bubble departure frequency.

It is shown that when the departure frequency is low, it increases with increasing Zuber number, or heat flux since the Zuber number is proportional to the heat flux. But when the departure frequency reaches a certain value, it will stop increasing. Sometimes the departure frequency even decreases slightly with increasing heat flux, for example, in Run 6. This phenomenon is caused by the bubble coalescence. When the bubble frequency is higher than 500 bubbles/s, bubble coalescence occurs close to a nucleation site, as shown in Fig. 5. When a bubble just departs from the nucleation site, its axial velocity is low, and its size grows. The second bubble at the nucleation site also grows. When they approach each other, the two bubbles may coalesce. It is shown in the images that the downstream bubble drags the bubble at the nucleation site, and that the diameter of the bubble at the nucleation site drops significantly. When bubble coalescence occurs at the nucleation site, it causes difficulties in counting the number of the bubbles departed. In the present study, some bubbles dragged by leading bubbles were not counted, which makes the counted frequency lower.

Bubble sliding phenomenon exists in subcooled boiling, as shown in Fig. 6. In the captured images, some bubbles do not lift-off when they depart from the nucleation cavity. They slide along the heater surface, and keep growing. The sliding bubbles might lift-off somewhere downstream of the cavity beyond the view of the image window.

It is also observed that bubble may collapse before it departs from the nucleation site. Some bubbles stay at the nucleation sites, and their size decreases from frame to frame. This suggests that these bubbles collapse before they depart from the nucleation cavity.

Furthermore, it is also indicated from the video images that the bubble departure frequency is not uniform. Some bubbles collapse before they depart from nucleation sites, some bubbles depart consecutively in a high frequency in a certain time interval. This suggests that the temperature distribution around the nucleation site is fluctuating, or in other words, the superheated

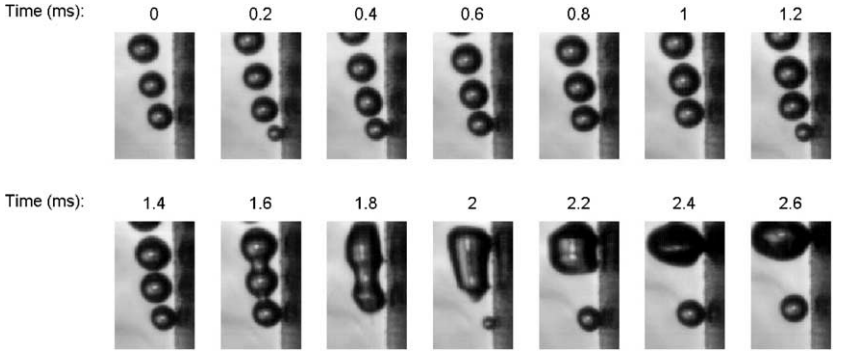

Fig. 5. Bubble coalescence for $T_{in} = 98.0$ °C, $q''_w = 59.8$, $v_{fi} = 0.595$ m/s, $z_d = 0.936$ m.

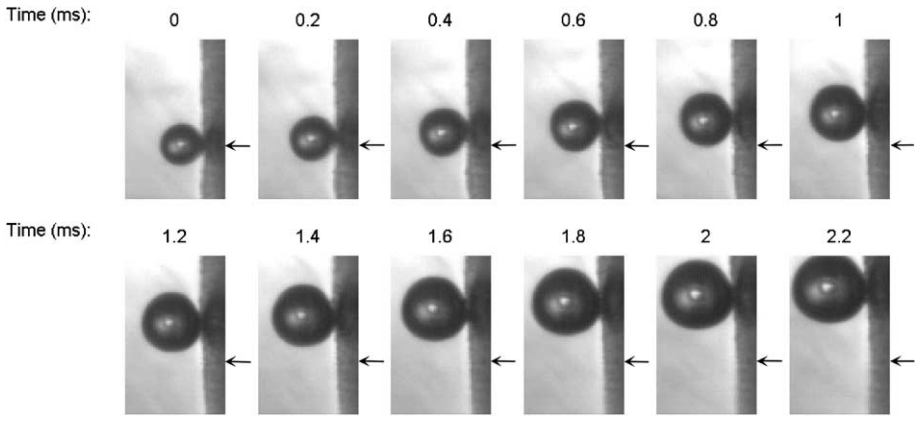

Fig. 6. Bubble sliding for $T_{in} = 98.0$ °C, $q''_w = 59.8$, $v_{fi} = 0.595$ m/s, $z_d = 0.936$ m (note: arrow point to the nucleation site position).

layer close to the heater surface dose not remain stable. When the superheated layer becomes thicker, bubbles will depart from the nucleation site; otherwise, these bubbles might collapse when they grow to a certain height.

3.3. Results of bubble lift-off diameter

A MATLAB program has been developed to analyze the digital images and to calculate the bubble diameter. The images were calibrated by taking photos of a set of stainless tubes with known diameters. The error caused by the light distortion is significantly reduced by adding the image box. The measurement error of bubble diameter can be estimated as the pixel distance, i.e., 11 μm.

In the data processing, the bubble lift-off diameter, instead of bubble departure diameter, was obtained. The first reason is that the bubble lift-off diameter can be used as the boundary condition for the bubble size transport equation, and the bubble departure diameter is not appropriate to act as the boundary condition. The second reason is the difficulty in defining the instant of bubble departure from the nucleation site.

In Runs 3 and 4, a few bubbles are out of the image window when they lift-off, and they have a large lift-off diameter, thus the accuracy of the averaged bubble lift-off diameter in such cases was reduced. However, such bubbles only account for less than 10% of the total captured bubbles; therefore, the error caused by these bubbles is not significant.

The bubble lift-off diameter is plotted for Runs 3, 4 and 6 against the bubble departure frequency in Fig. 7. For Run 3, bubble lift-off diameter decreases with the increase of the bubble departure frequency. In pool boiling, as discussed in the Section 1, researchers also found that bubble departure size decreases while increasing the departure frequency. Warrier et al. [16] measured the bubble departure frequency and bubble

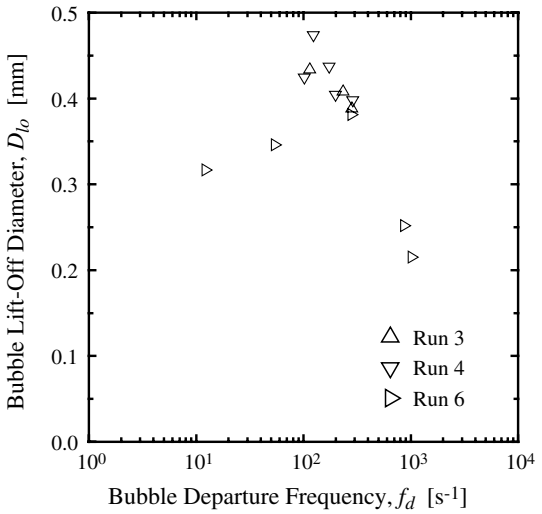

Fig. 7. Results of bubble lift-off diameter against bubble departure frequency.

lift-off diameter in forced convection flow boiling, and observed the same trend as Run 3.

However, in Runs 4 and 6, the bubble lift-off diameter first increases, and then decreases with the increase of the bubble departure frequency. One possible reason is: The heat surface temperature fluctuates during a nucleation cycle due to the effect of micro-layer underneath the growing bubble. The wall temperature decreases when a bubble appears and grows at the nucleation site, and then increases after the bubble departs. This can be defined as a wall temperature fluctuation cycle. The wall temperature cycle is the same as the nucleation cycle. When bubble departure frequency is relative high, i.e., higher than 100 bubbles/s, a new wall temperature cycle begins right after the wall temperature return to the original value. For such cases, bubble lift-off size may have a close relationship to the bubble

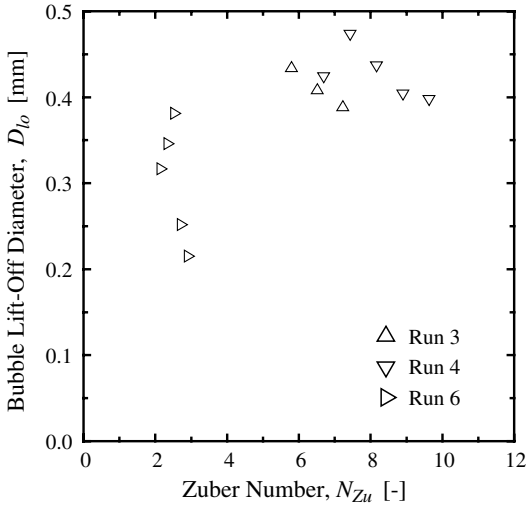

Fig. 8. Results of bubble lift-off diameter against Zuber number.

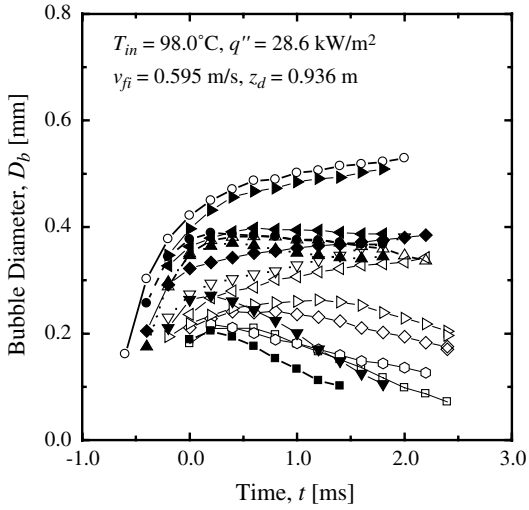

Fig. 9. Evolution of bubble diameter.

departure frequency. Otherwise, when the bubble departure frequency is low, i.e., smaller than 100 bubbles/s, the bubble waiting period is relatively long, and wall temperature returns to the original value before the next nucleation cycle begins. In such cases, the bubble lift-off size may not be considerably related to bubble departure frequency. More data are needed to validate this point.

Fig. 8 show the relationship between bubble lift-off diameter and the Zuber number. The trend in Fig. 8 is the same as those in Fig. 7 because bubble departure frequency increases as the increase of Zuber number.

3.4. Results of bubble dynamics after lift-off

The bubble sizes after lift-off are calculated for one test point in Run 6. Several typical trends of bubble diameter evolutions are shown in Fig. 9. The local bulk temperature in Fig. 9 is higher than 99 °C and very close to the saturation temperature. The time "0" represents the moment when bubbles lift-off. The negative time represents a moment before bubbles lift-off. It can be clearly seen from this figure that after lift-off some bubbles are condensed, some bubbles first grow and then are condensed, and some bubbles continue to grow. The reason of these phenomena is the fluctuation of the local temperature. If the bulk temperature is lower, bubbles will be condensed; otherwise, bubbles will grow.

The averaged growth rate of the bubble diameter is shown in Fig. 10 for the same condition as in Fig. 9. The definitions of the x-coordinate are also the same as those in Fig. 9. The error bars shows the standard deviations of the data. The curve shows that the bubble diameter grows significantly before lift-off. However, the bubble

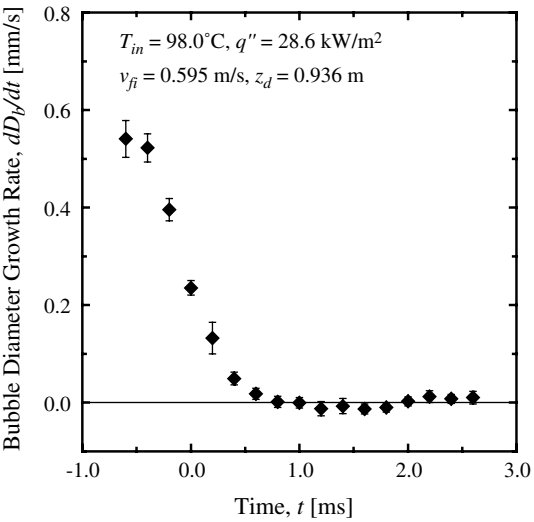

Fig. 10. Evolution of averaged bubble diameter growth rate.

growth rate decreases sharply with time (the bubble diameters in the early growth period are too small to be measured). After the bubbles lift off, the growth rate drops gradually to zero, and the averaged bubble diameter does not decrease significantly for after 2.0 ms. This is because that the bulk subcooling is very small and the bubbles are very close to the heater wall. When the bubbles enter the subcooled bulk core region, the bubble growth rate will be negative. This is not shown in the figure because of the size limit of the image window.

The average distance from the wall to the bubbles after lift-off is shown in Fig. 11. It suggests that after

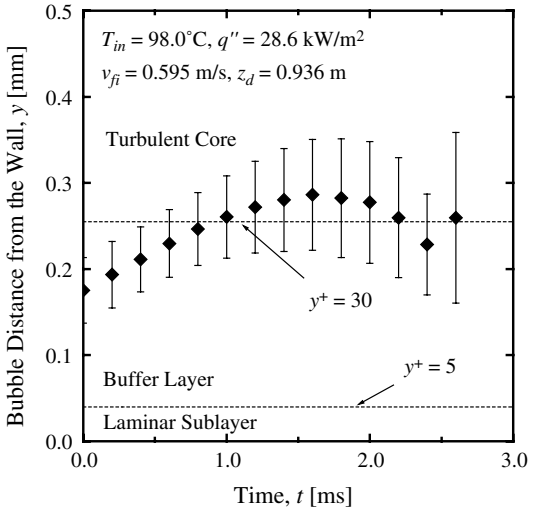

Fig. 11. Evolution of averaged bubble distance from the wall.

bubble lift-off, bubbles first move against the wall, and then move towards the wall.

The average bubble axial velocity is shown in Fig. 12, which is of the same case as in Fig. 11. Fig. 12 also shows the corresponding liquid axial velocity, which is estimated by the following empirical formula [17]:

$$\begin{cases} \text{Laminar sublayer } (0 \leqslant y^+ \leqslant 5) : v^+ = y^+ \\ \text{Buffer layer } (5 \leqslant y^+ \leqslant 30) : v^+ = -3.05 + 5.00 \ln y^+ \\ \text{Turbulent core } (y^+ \leqslant 30) : v^+ = 5.5 + 2.5 \ln y^+ \end{cases} \tag{3}$$

where v^+ and y^+ are non-dimensional velocity and distance, respectively. The distances shown in Fig. 11 are used.

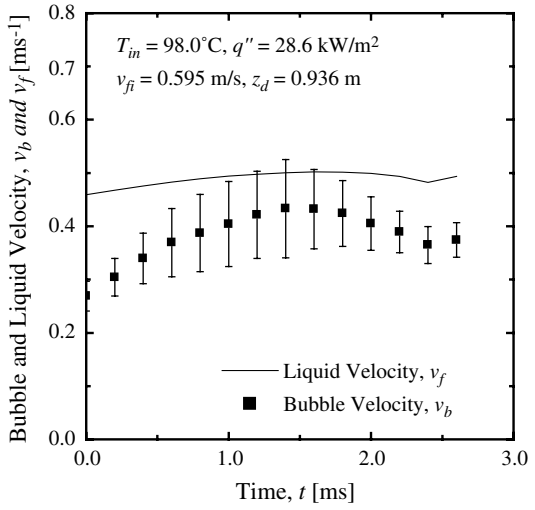

Fig. 12. Evolution of averaged bubble axial velocity and the corresponding estimated liquid axial velocity.

Fig. 12 shows that after bubbles lift-off, bubbles first accelerate, and then decelerate, which agrees well with Fig. 11. It is interesting that the liquid velocity is higher than the bubble velocity during the 2.6 ms period after lift-off. At the moment of lift-off, the bubble velocity may not be zero because bubbles slide before lift-off. After lift-off, bubbles are pushed by the liquid, accelerate and move towards the turbulent core. At about 1.4 ms, bubbles are pushed back by turbulence and move towards the wall. At this moment bubbles are moving along the transition between buffer layer and the turbulent core, as shown in Fig. 11. When bubbles move closer to the wall, the liquid velocity decreases, and this causes the decrease of the bubble velocity. The averaged bubble velocity is lower than the liquid velocity, which suggests that bubbles are accelerated by the liquid.

4. Conclusions

Forced convection subcooled water boiling experiments were conducted on an annular channel with upward flow. A high-speed digital video camera (5000 fps) was applied to record the dynamics of the subcooled ebullition process. The video images show that the bubble waiting period varies significantly in different nucleus cavities and different experimental conditions, while the bubble growth period is relatively stable and short, i.e., less than 3 ms. Generally the bubble departure frequency increases as the heat flux increases. Bubble coalescence occurs at the nucleation site when the bubble frequency is higher than 500 bubbles/s. For some cases, the departure frequency reaches an asymptotic limit near 1000 bubbles/s.

The averaged bubble lift-off diameters, bubble growth rate and velocity after lift-off were also measured by analyzing the images. The averaged bubble growth rate drops sharply after lift-off. Bubble growth or condensation is determined by the distance between the bubble and the heated wall. In a few milliseconds after lift-off, the averaged bubble axial velocity is smaller than the liquid velocity, which implies that bubbles are accelerated by the liquid.

Acknowledgements

The authors would like to acknowledge the support by Tokyo Electric Power Company.

References

[1] M. Ishii, Thermo-Fluid Dynamics Theory and Two-Phase Flow, Eyerolles, Paris, 1975.
[2] G. Kocamustafaogullari, M. Ishii, Foundation of the interfacial area transport equation and its closure relations, Int. J. Heat Mass Transfer 38 (1995) 481–493.

[3] G. Kocamustafaogullari, M. Ishii, Interfacial area and nucleation site density in boiling systems, Int. J. Heat Mass Transfer 26 (1983) 1377–1387.
[4] J.R. Riznic, M. Ishii, Bubble number density and vapor generation in flashing flow, Int. J. Heat Mass Transfer 32 (1989) 1821–1833.
[5] M. Jocob, in: Heat Transfer, Vol. I, Wiley, New York, 1949.
[6] N. Zuber, Nucleate boiling: the region of isolated bubbles and the similarity with natural convection, Int. J. Heat Mass Transfer 6 (1963) 53–78.
[7] J.T. Rogers, M. Salcudean, Z. Abdullah, D. Mcleod, D. Poirier, The onset of significant void in up-flow boiling of water at low pressure and velocities, Int. J. Heat Mass Transfer 30 (1987) 2247–2260.
[8] S.C. Lee, S.G. Bankoff, A comparison of predictive models for the onset of significant void at low pressures in forced-convection subcooled boiling, KSME Int. J. 12 (1998) 504–513.
[9] F.C. Gunther, Photographic study of surface-boiling heat transfer to water with forced convection, Trans. ASME 73 (1951) 115–124.
[10] H.C. Unal, Void fraction and incipient point of boiling during the subcooled nucleate flow boiling of water, Int. J. Heat Mass Transfer 20 (1977) 409–419.
[11] O. Zeitoun, M. Shoukri, V. Chatoorgoon, Measurement of interfacial area concentration in subcooled liquid–vapour flow, Nucl. Eng. Des. 152 (1994) 243–255.
[12] S.G. Kandlikar, B.J. Stumm, A control volume approach for investigating forces on a departing bubble under subcooled flow boiling, in: Fundamentals of Phase Change: Boiling and Condensation, ASME HTD, vol. 273, 1994, pp. 73–80.
[13] G.E. Thorncroft, J.F. Klausner, R. Mei, An experimental investigation of bubble growth and detachment in vertical upflow and downflow boiling, Int. J. Heat Mass Transfer 41 (1998) 3857–3871.
[14] G.R. Warrier, N. Basu, V.K. Dhir, Interfacial heat transfer during subcooled flow boiling, Int. J. Heat Mass Transfer 45 (2002) 3947–3959.
[15] M. Bartel, M. Ishii, T. Masukawa, Y. Mi, R. Situ, Interfacial area measurements in subcooled flow boiling, Nucl. Eng. Des. 210 (2001) 135–155.
[16] G.R. Warrier, N. Basu, V.K. Dhir, Subcooled boiling at low pressures, Annual Progress Report for USNRC Task Order No. 5, UCLA ENG-99-211, 1999.
[17] L.M.K. Boelter, R.C. Martinelli, F. Jonassen, Remarks on the analogy between heat transfer and momentum transfer, J. Heat Transfer 63 (1941) 447–455.